Supplementary Information

Mesoporous Ni-doped $MnCo_2O_4$ Hollow Nanotubes as Anode Material of Sodium Ion Battery with Ultralong Life and Pseudocapacitive Mechanism

Lijun Wu,[a,b] Junwei Lang,[a] Peng Zhang,[a,b] Xu Zhang,[a] Ruisheng Guo,[a] Xingbin Yan*[a]

[a] Laboratory of Clean Energy Chemistry and Materials, State Key Laboratory of Solid Lubrication, Lanzhou Institute of Chemical Physics, Lanzhou 730000, P. R. China.

[b] University of Chinese Academy of Sciences, Beijing, 100039, P.R. China.

* Corresponding author. Tel.: +86-931-4968055; Fax: +86-931-4968055.

E-mail address: xbyan@licp.cas.cn

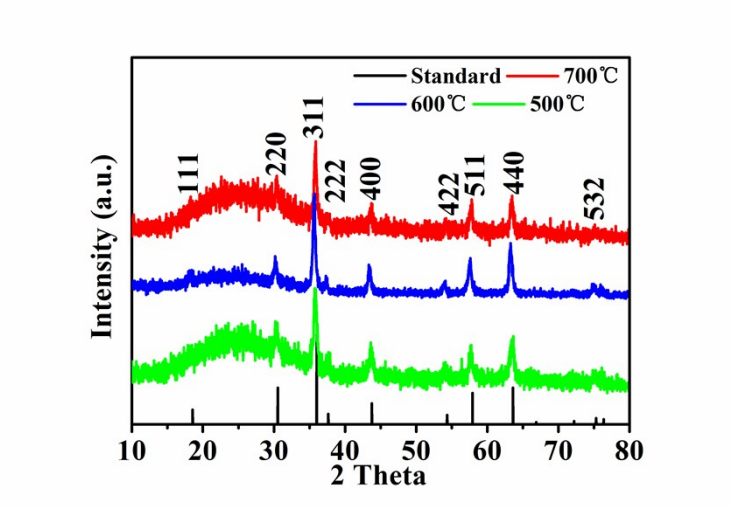

Figure S1. XRD patterns of the as-prepared MCNO-HNTs at different calcining temperatures;

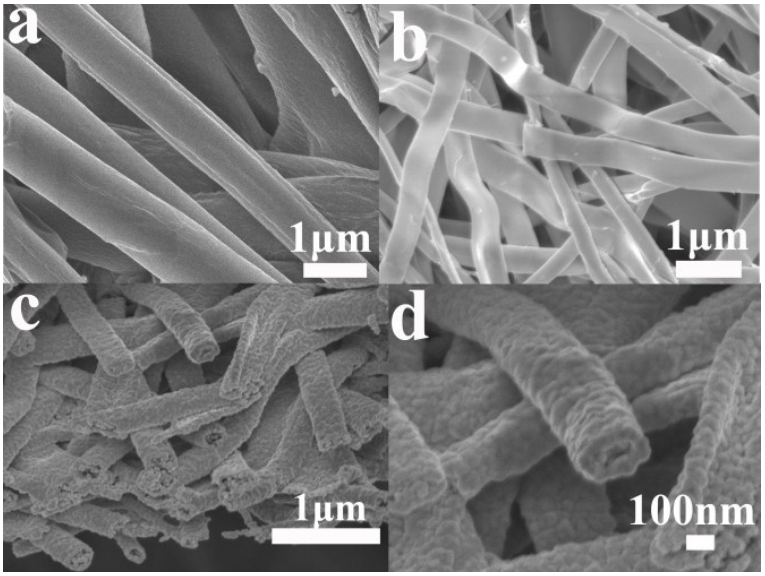

Figure S2. (a), (b) FESEM images of the precursor fibers of as-prepared MCNO-HNTs and PNBs; (c), (d) Low and high magnification FESEM images of as-prepared MCNO-PNBs.

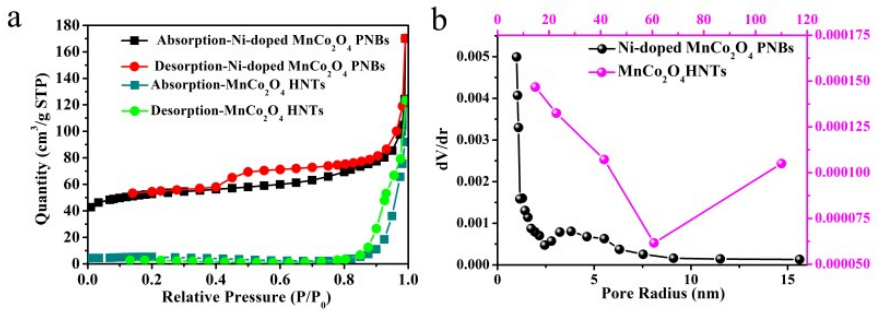

Figure S3. (a) The absorption-desorption isotherms and (b) Pore size distributions of MCNO-PNBs and MCO-HNTs.

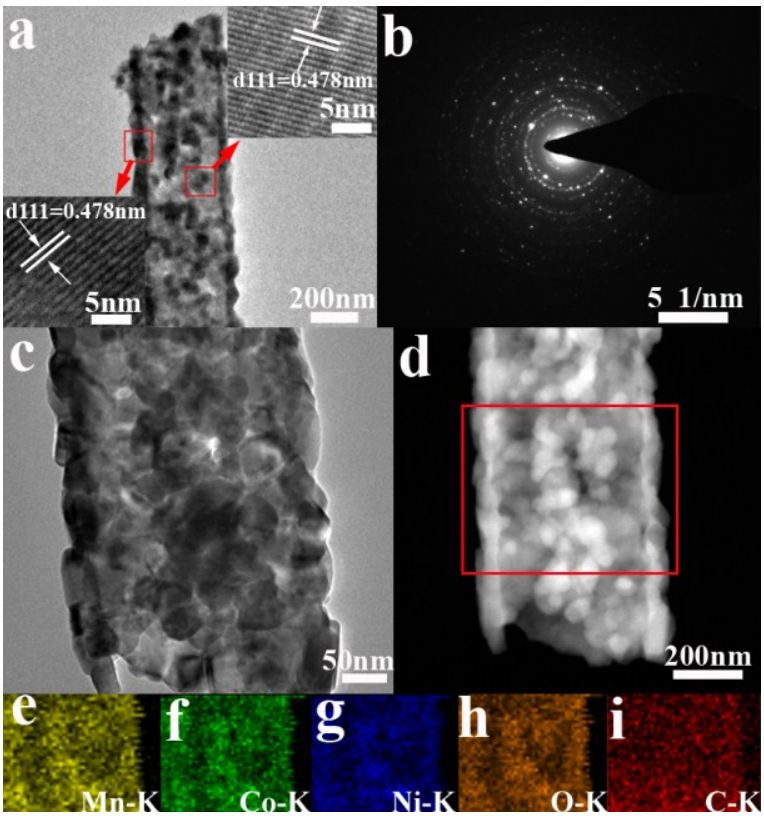

Figure S4. (a) Low magnification TEM image of as-prepared MCNO-PNBs, (b) Selected area electron diffraction (SAED) pattern, (c) The representative bright-field TEM image, (d) Annual dark-field TEM (ADF-TEM) image of an individual MCNO-PNBs and the corresponding element mappings: (e) Mn, (f) Co, (g) Ni, (h) O and (j) C.

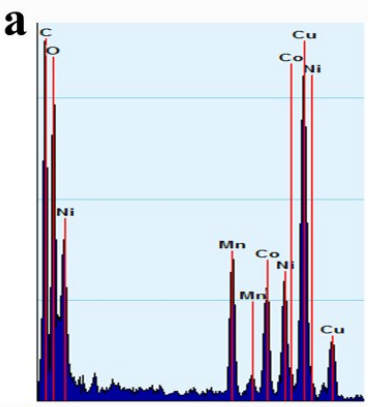

b

Element	Atom (wt%)	Atom ratio (mol)
Mn	4.4	1.03
Co	4.7	1
Ni	4.7	1
O	5.15	4.02

Figure S5. (a), (b) EDX spectrum and the atomic ratio of Co, Mn and Ni three elements of MCNO-HNTs.

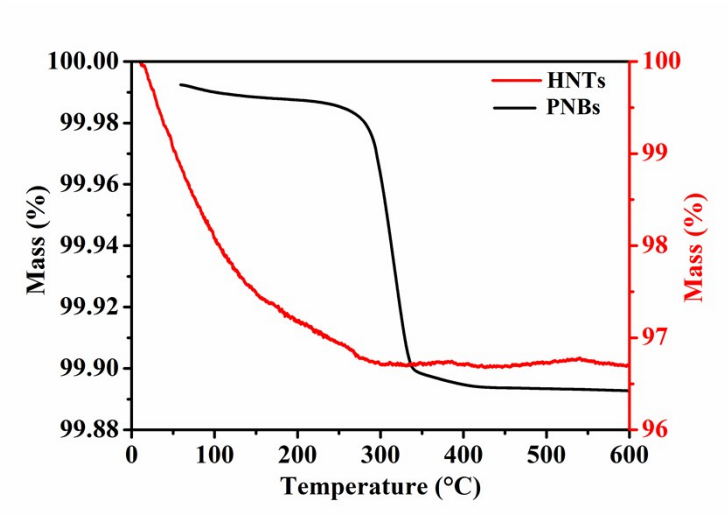

Figure S6. TG curves of as-prepared MCNO-HNTs and PNBs.

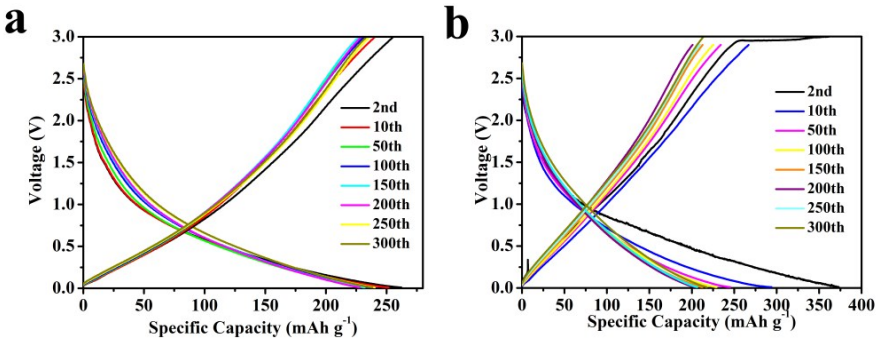

Figure S7. (a), (b) The profiles of voltage *vs* specific capacity for mesoporous MCNO-HNTs and MCNO-PNBs *vs* Na/Na^+ at 0.01-3.0 V for the different cycles.

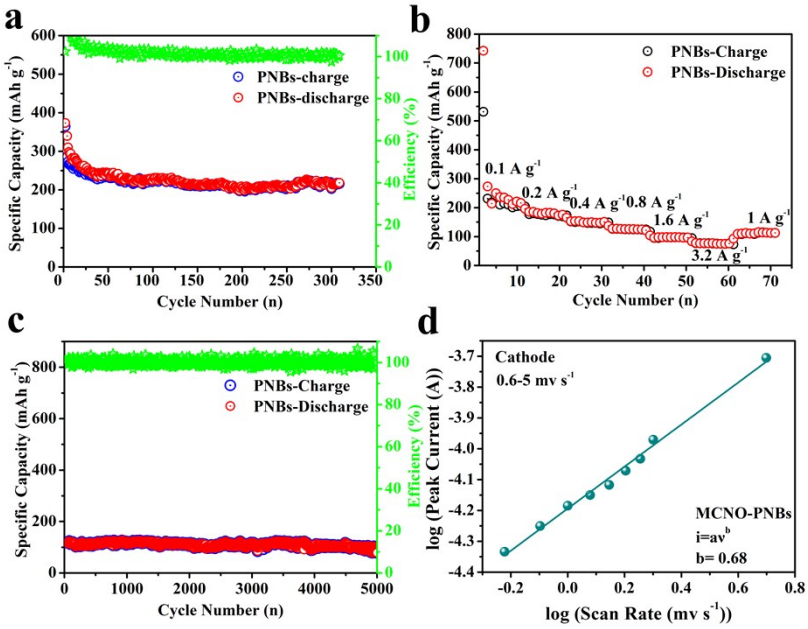

Figure S8. (a) Cyclic performance for MCNO-PNBs *vs* Na/Na^+ at 0.1 A g^{-1} for 325 cycles, (b) Capacity evolution of MCNO-PNBs by varying charge/discharge rates ranging from 0.1, 0.2, 0.4, 0.8, 1.6, 3.2 A g^{-1} and back to 0.1 A g^{-1}, (c) Cyclic performance after the testing of rate capability at different current densities in Figure S8b for MCNO-PNBs *vs* Na/Na^+ for 5000 cycles at 1 A g^{-1}, (d) The b-value determination of the peak currents of cathode shows that charge storage of MCNO-PNBs *vs* Na/Na^+.

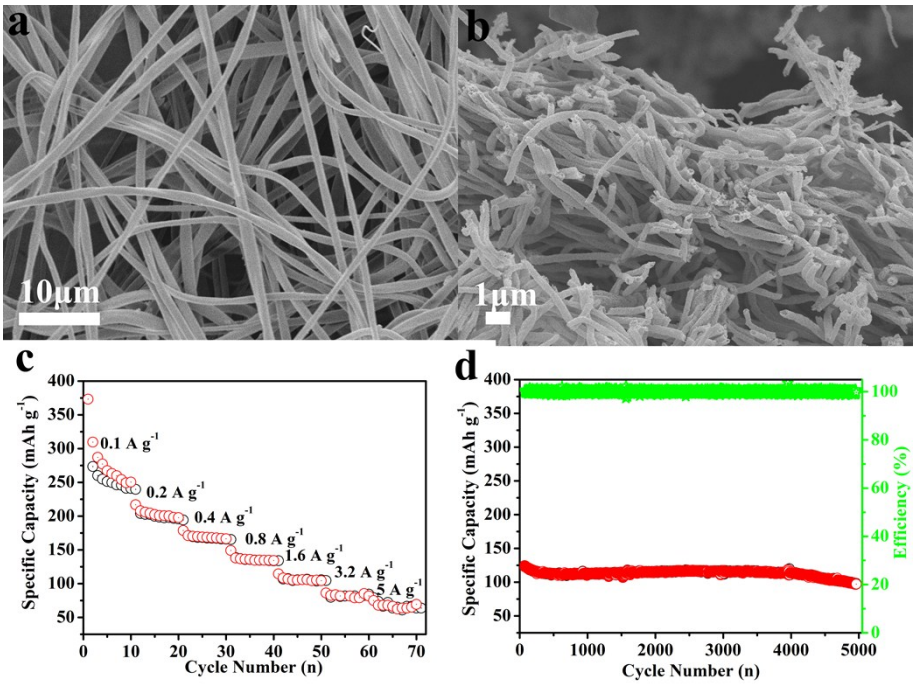

Figure S9. (a) Low magnification FESEM images of the precursor fibers of MCO-HNTs, (b) Low magnification FESEM images of MCO-HNTs, (c) Rate characteristic of MCO-HNTs *vs* Na/Na^+, (d) Cyclic performance after the testing of rate capability at different current densities in Figure S9c for MCO-HNTs *vs* Na/Na^+ for 5000 cycles at 1 A g^{-1}.

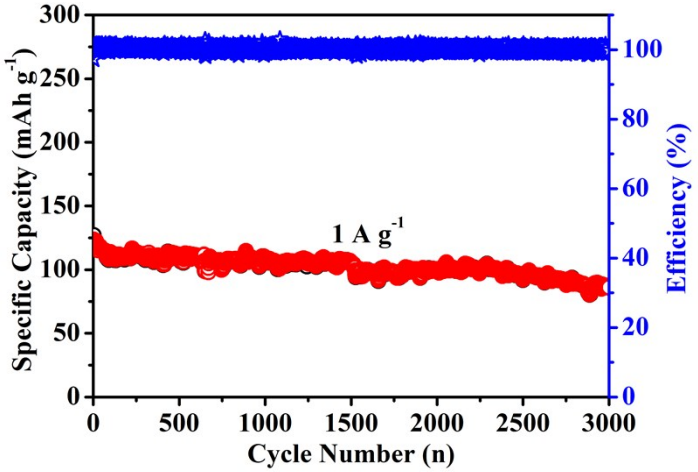

Figure S10. Cyclic performance with non-activated process of the MCNO-HNTs *vs* Na/Na^+ for 3000 cycles at 1 A g^{-1}.

Table S1 A summary of recent studies on transition metal oxides anode materials for SIBs.

Materials	Voltage range (V)	Current density (mA g^{-1})	Capacity (mA h g^{-1})	Cycle number	Ref
$MnFe_2O_4$@C nanofibers	0.01-3	100	500	After 300	1
		1000	391	After 4200	
		10000	305		
Metal organic frameworks derived hierarchical hollow NiO/Ni/graphene composites	0.005-3	200	385		2
		1000	Less 200	200	
		2000	207		
Fe_3O_4 and Co_3O_4 nanocrystals encapsulated in carbon microspheres	0.001-3	100 (F_3O_4)	513	60	3
		500	309	100	
		2000	246		
		5000	163		
		100 (Co_3O_4)	583		
		500	228	150	
		2000	183		
carbon-coated Fe_3O_4	0-2	200	~160	50	4
		2000	157		
$NiCo_2O_4$ nanowire arrays	0.01-3	50	542	50	5
		400	363	20	
Fe_2O_3-rGO composite powders	0.001-3	300	174	200	6
Fe_2O_3@GNS	0.005-3	200	327		7
		1000	166	100	
		5000	154		
Fe_2O_3 film	0.005-3	100	386	200	8
		200	331	200	
		1000	273	200	
		5000	233		
G-TiO_2	0.05-3	50	265		9
		1500	125		
		6000	102		
		500	120	After 4300	
Nanostructured iron oxide	0.05-2.8	250	130	60	10
Co_3O_4 anchored carbon nanotubes	0.01-3	50	403	100	11
		1600	212		
		3200	190		
Ultrafine niobium oxide nanocrystals/reduced graphene oxide (Nb_2O_5 NCs/rGO)	0-3	100	110	100	12

			1000	170		
			5000	115		
mesoporous Nb_2O_5/carbon composite		0.01-2.5	50	175		13
			100	-	300	
			1000	60		
SnO_2@3DG		0.01-3	100	432	200	14
			800	210		
rGO@TiO_2 NFs			67	217		15
			670	146		
			3350	87		
Binder-free porous CuO arrays		0-3	200	290.6	450	16
This work	MCNO-HNTs	0.01-3	100	238.6	After 700	
			1600	129.1		
			5000	98.8		
			1000	109 (81%)	After 11000	
	MCNO-PNBs		100	269.9		
			1600	114.5		
			1000	103 (85.8%)	After 5000	

1. Y. Liu, N. Zhang, C. Yu, L. Jiao and J. Chen, *Nano lett.,* 2016. **16**, 3321-3328.
2. F. Zou, Y. M. Chen, K. Liu, Z.Yu, W. Liang, S. M. Bhaway, M. Gao and Y. Zhu, *ACS nano,* 2016**, 10**, 377-386.
3. Y. Zhou, W. Sun, X. Rui, Y. Zhou, W. J. Ng, Q. Yan and E. Fong, *Nano Energy,* 2016**, 21,** 71-79.
4. S. M. Oh, S. T. Myung, C. S. Yoon, J. Lu, J. Hassoun, B. Scrosati, K. Amine and Y. K. Sun, *Nano lett.,* 2014**, 14**, 1620-1626.
5. Y. Mo, Q. Ru, J. Chen, X. Song, L. Guo, S. Hu and S. Peng, *J. Mater. Chem. A,* 2015**, 3**, 19765-19773.
6. G. D. Park, J. S. Cho, J. K. Lee and Y. C. Kang, *Sci. Rep.,* 2016**, 6**, 22432-22442.
7. W. Sun, X. Rui, J. Zhu, L.Yu, Y. Zhang, Z. Xu, S. Madhavi and Q.Yan, *J. Power Sources,* 2015**, 274**, 755-761.
8. Y. Jiang, M. Hu, D. Zhang, T. Yuan, W. Sun, B. Xu and M. Yan, *Nano Energy,* 2014**, 5,** 60-66.
9. C. J. Chen, Y. W. Wen, X. L. Hu, X. L. Ji, M. Y. Yan, L. Q. Mai, P. Hu, B. Shan and Y. H. Huang, *Nat. Commun.,* 2015**, 6,** 6929-6937.
10. M. Valvo, F. Lindgren, U. Lafont, F. Björefors and K. Edström, *J. Power Sources*, 2014, **245**, 967-978.
11. Md M. Rahman, I. Sultana, Z. Q. Chen, M. Srikanth, L. H. Li, X. J. Dai and Y. Chen, *Nanoscale*, 2015, **7**, 13088-13095.
12. L. T. Yan, G. Chen, S. Sarker, S.Richins, H. Q. Wang, W. C. Xu, X. H. Rui and H. M. Luo, *ACS Appl. Mater. Interfaces,* 2016, **8**, 22213-22219.
13. H. Kim, E. Lim, C. Jo, G. Yoon, J. Hwang, S. Jeong, J. Lee and K. Kang, *Nano Energy*, 2015, **16**, 62-70.
14. L. Pei, Q. Jin, Z. Zhu, Q, Zhao, J. Liang and J. Chen, *Nano Res.*, 2015, **8**, 184-192.
15. Y. Yeo, J-W Jung, K. Park and Il-D. Kim, *Sci Rep*., 2015, **5**, 13862-13971.
16. S.Yuan, X. Huang, D. Ma, H. Wang, F. Meng and X. Zhang, *Adv. Mater*., 2014, **26**, 2273-2279.

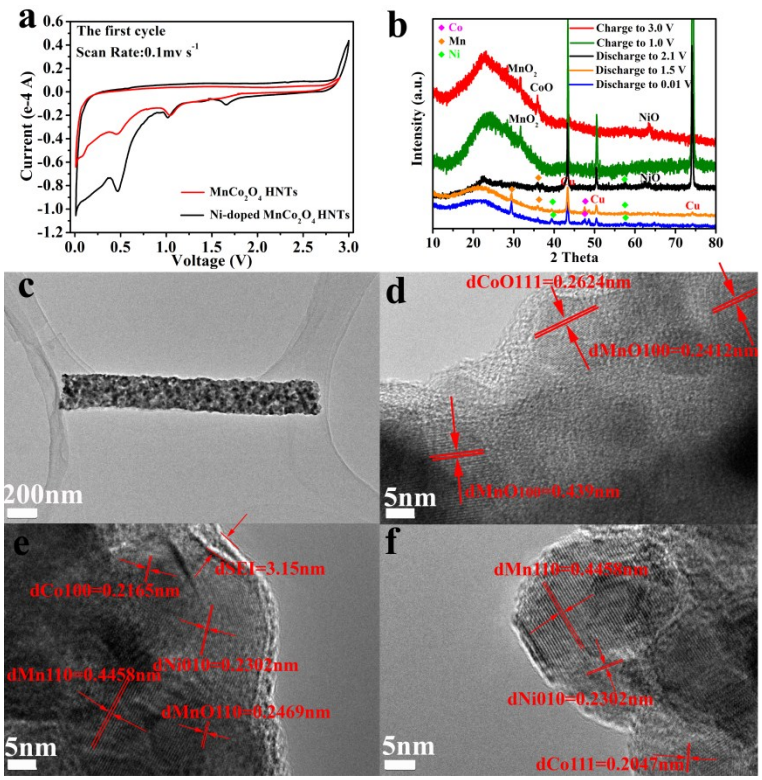

Figure S11. (a) Cyclic voltammetry curves for the first cycle of MCNO-HNTs and MCO-HNTs *vs* Na/Na^+, (b) Ex-situ XRD pattern of MCNO-HNTs at different charge and discharge voltage, MnO_2 in the figure is the charge product-MnO that is oxidized in the air. (c)-(f) TEM and HRTEM images of MCNO-HNTs at fully second charge voltage (3.0 V), discharge voltage (1.5 V) and completely discharge voltage (0.01 V).

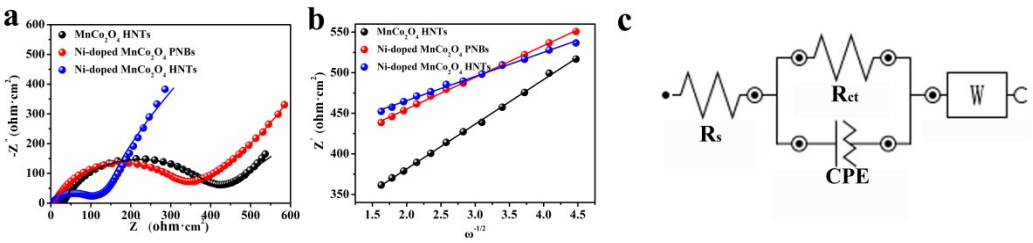

Figure S12. (a) Nyquist dots of the MCNO-HNTs, MCNO-PNBs and $MnCo_2O_4$ HNTs , (b) Real parts of the impedance (Z') versus the reciprocal square root of angular frequency (ω) in the low frequency region of the above samples mentioned.

Figure S11a presents the electrochemical impedance spectroscopy (EIS) responses of the typical the MCNO-HNTs, MCNO-PNBs and $MnCo_2O_4$ HNTs samples. All the Nyquist plots are composed of a depressed semicircle from high to medium frequency followed by a slope line in the low frequency region. Where the former is related to the charge-transfer process (R_{ct}) at the electrode/electrolyte interfaces, the latter corresponds to the Warburg impedance (Z_w) associated with Na^+ diffusion in the fibrous $MnCo_2O_4$ framework. R_s refers to the solution resistance, and constant-phase element (CPE) represents the double-layer capacitance, taking into account the roughness of the particle surface.

Table S2. Simulated impendence parameters (*Rs*, *Rct*) and calculated Warburg factor (σ) of the MCNO-HNTs, MCNO-PNBs and MCO-HNTs samples.

Samples	**R_s (Ω)**	**R_{ct} (Ω)**	**σ**
MCNO-HNTs	4.5	114	29.7
MCNO-PNBs	5.5	364	39.8
MCO-HNTs	28.9	428	55.1

As can be seen from the simulation results summerized in Table S2, MCNO-HNTs possess the smaller R_{ct} and R_s values than MCO-HNTs. This indicates that the Ni-doping can enhance the electronic conductivity of the composite. EIS is also an important tool to evaluate the diffusion coefficient of Na^+ ions (D_{Na}) within the electrode:

$$D_{Na} = \frac{R^2T^2}{2A^2n^4F^4C^2\sigma^2} \qquad (1)$$

In eq (1), R is the gas constant, T is the absolute temperature, A is the surface area of electrode, n is the number of electrons per molecule during oxidization, F is the Faraday constant, C is the concentration of sodium ion, and σ is the Warburg factor, σ relates to Z' through eq (2) and its value can be obtained from the slope of the line between Z' and $\omega^{-1/2}$ as shown in Figure S9b.[3,4]

$$Z' = R_s + R_{ct} + \sigma\omega^{-1/2} \qquad (2)$$

As can be calculated, the σ value of the MCNO-HNTs is the smallest (Table S1), reflecting the largest D_{Na}. This further demonstrates that the Ni-doping can facilitate the Na^+ ions diffusion kinetics.

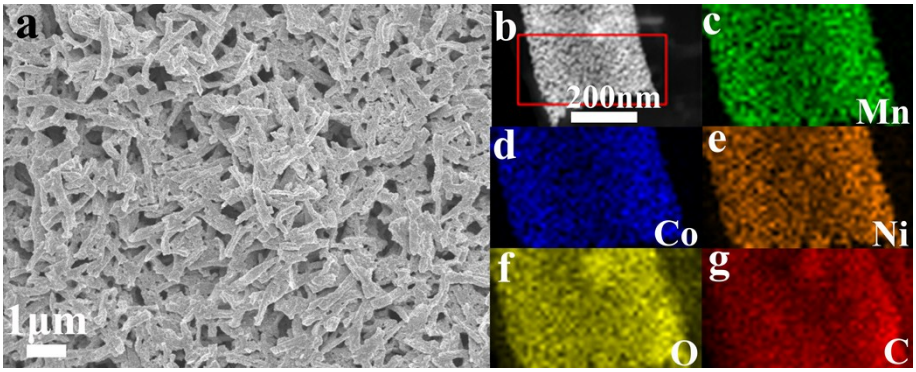

Figure S13. (a) SEM and (b) TEM, EDS mapping images of MCNO- HNTs *vs* Na/Na^+ after 500 cycles.

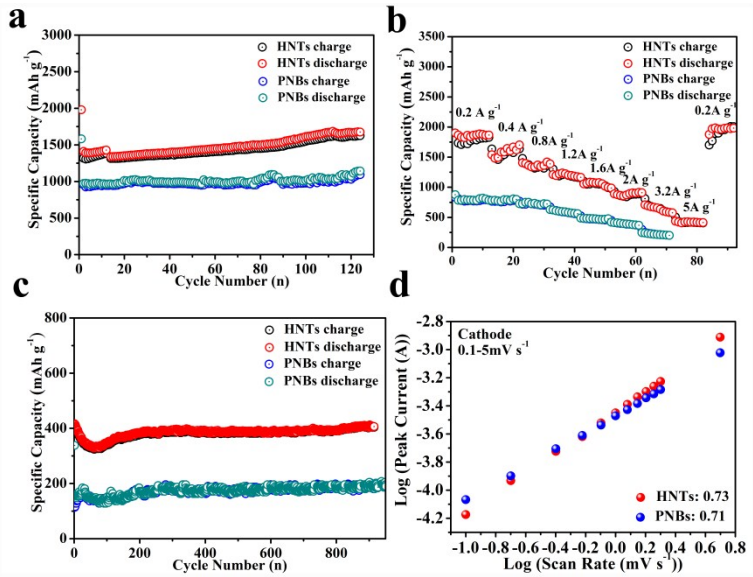

Figure S14. (a) Cycling performances for MCNO-HNTs and PNBs *vs* Li/Li^+ at 0.1 A g^{-1} for 150 cycles, (b) Rate characteristic of MCNO-HNTs and PNBs *vs* Li/Li^+, (c) Cycling performances for MCNO-HNTs and PNBs *vs* Li/Li^+ for 1000 cycles at 5 A g^{-1}, (d) The b-value determination of the peak currents of cathode shows that charge storage of MCNO-HNTs and PNBs *vs* Li/Li^+.